Expanded View Figures

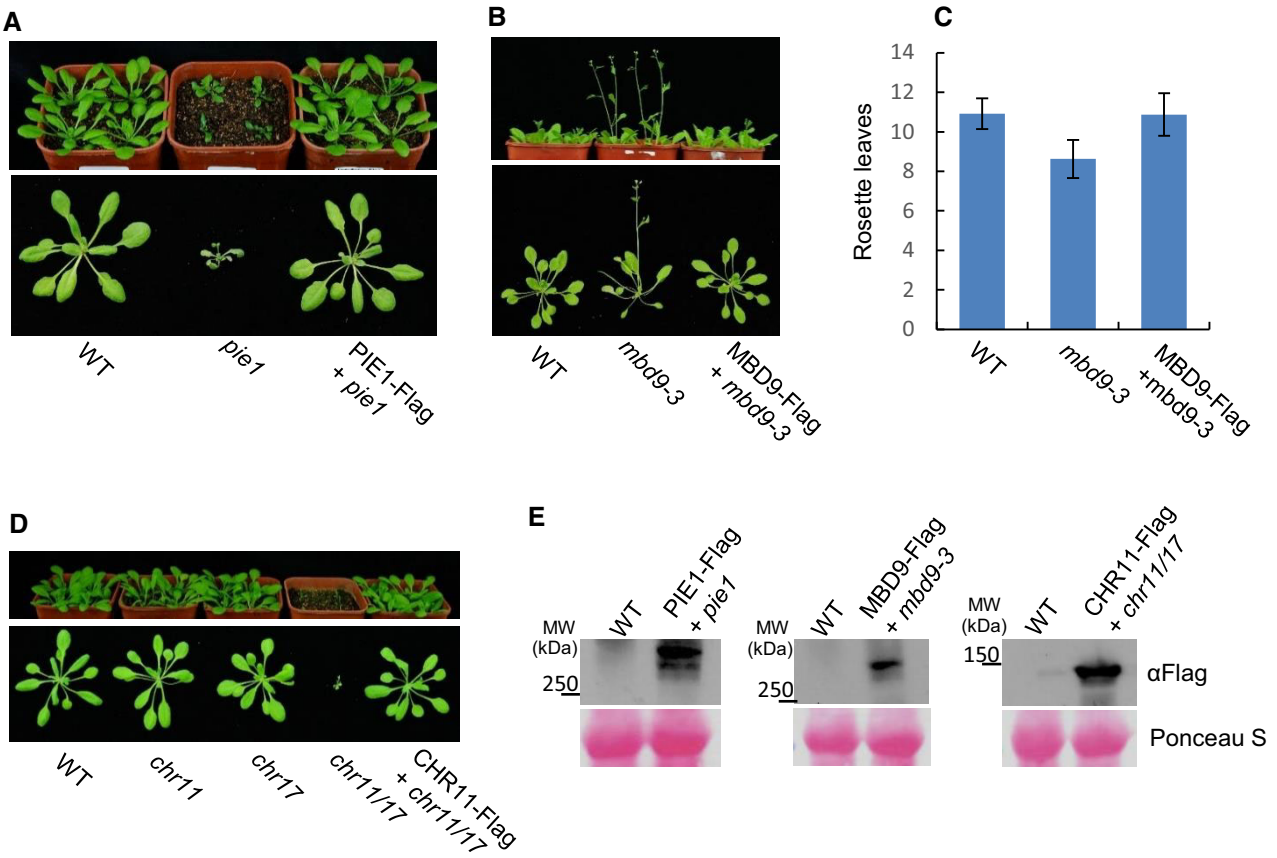

Figure EV1. The complementation test of the SWR1 complex mutants *mbd9-3*, *pie1*, and *chr11/17*.

A The complementation test of the *pie1* mutant. The top and bottom panels show morphological phenotypes of 24-day-old plants in the soil and on the black cloth, respectively.

B The complementation test of the *mbd9-3* mutant. Shown are morphological phenotypes of 24-day-old plants in the soil (the top panel) and on the black cloth (the bottom panel).

C Numbers of rosette leaves of the WT, *mbd9-3*, and *MBD9-Flag* transgenic plants in the *mbd9-3* background. At least 20 plants of each genotype were counted. Values are mean ± SD.

D The complementation test of the *chr11/17* mutant. The developmental defect of the *chr11/17* mutant was complemented by CHR11-Flag. The top and bottom panels show the phenotypes in the soil and on the black cloth, respectively.

E Verification of the expression of MBD9-Flag, PIE1-Flag, and CHR11-Flag in each transgenic line. The top panel is the Western blot results of the expression of these three transgenes. The bottom is the corresponding *Ponceau S* staining loading control.

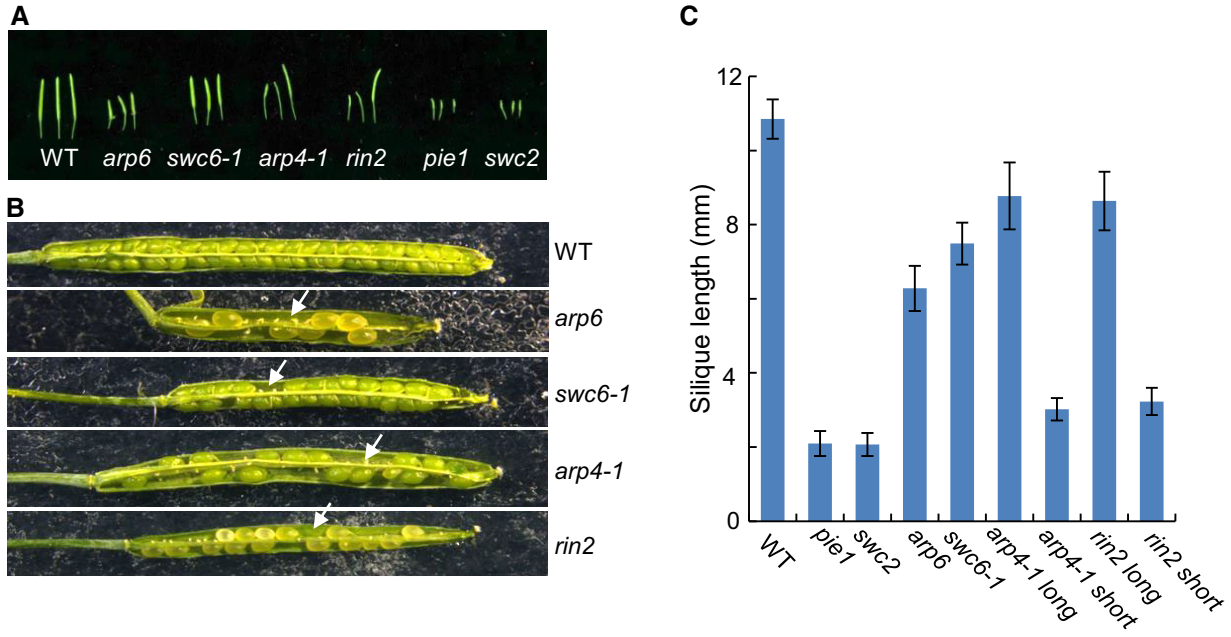

Figure EV2. The morphological phenotypes of reproductive organs in the WT and SWR1 complex mutants.

A Siliques of WT, *arp6*, *swc6-1*, *arp4-1*, *rin2*, *pie1*, and *swc2*. In the *arp4-1* and *rin2* mutants, there are two different types of siliques. One is similar to that in the WT and the other is shorter than that in the WT. Both types of siliques are shown.

B Open siliques of WT, *arp6*, *swc6-1*, *arp4-1*, and *rin2*. Arrowheads indicate aborted ovules. Long siliques of *arp4-1* and *rin2* are shown.

C Average silique length of WT, *arp6*, *swc6-1*, *arp4-1*, and *rin2*. At least 20 siliques were calculated for each mutant. Values are mean ± SD. "*arp6* long" and "*rin2* long" stand for the long siliques of *arp6* and *rin2* mutants, while "*arp6* short" and "*rin2* short" stand for the short siliques of these two mutants.

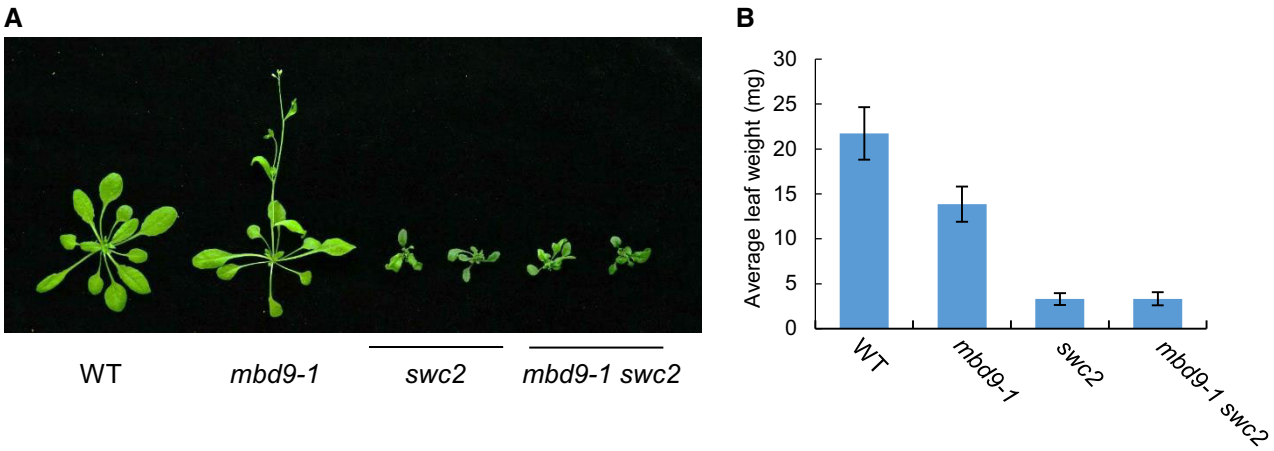

Figure EV3. The developmental defect of the *swc2* mutant is comparable to that of the *mbd9-1 swc2* double mutant.

A The morphological phenotype of WT, *mbd9-1*, *swc2*, and *mbd9-1 swc2*. Shown are 24-day-old plants.

B Average leaf weight of WT, *mbd9-1*, *swc2*, and *mbd9-1 swc2*. For each plant, the total leaf weight and leaf number were recorded and the average leaf weight of each plant was calculated. Only rosette leaves were used for the analysis. At least 20 plants were used for each sample. Values are mean ± SD.

A

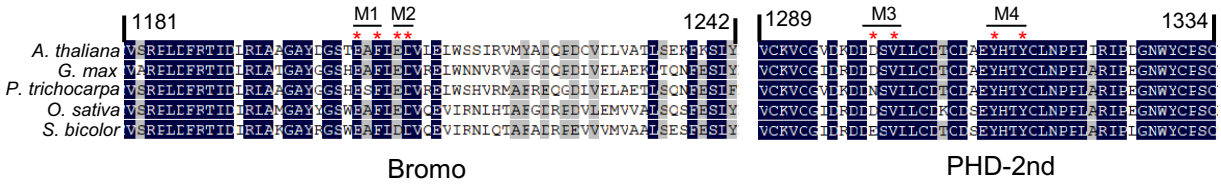

B

MBD9 mutant constructs	Mutation Sites			
	M1 (E1204A,F1206A)	M2 (E1208A,D1209A)	M3 (D1300A,V1302A)	M4 (Y1312A,Y1315A)
FL				
M1	√			
M2		√		
M1M3	√		√	
M1M4	√			√
M2M3		√	√	
M2M4		√		√

C

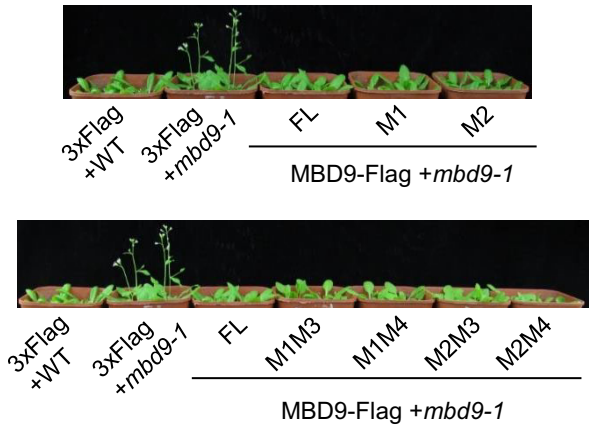

D

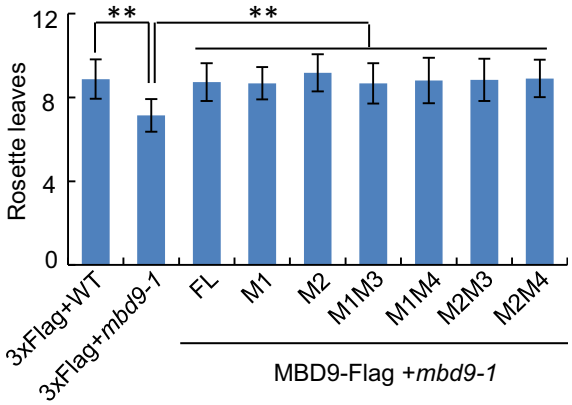

Figure EV4. Mutations of conserved residues in the BROMO and the second PHD domains of MBD9 do not affect the biological function of MBD9.

A Shown are mutation sites in the BROMO domain and the second PHD domain of MBD9. The alignment of MBD9 and its plant orthologs is shown.

B Shown are MBD9 mutation sites in each of the complementary transgenic lines in the *mbd9-1* mutant background.

C The flowering-time phenotypes of WT, *mbd9-1*, and the complementary transgenic lines harboring WT and mutated *MBD9* transgenes.

D The number of rosette leaves of WT, *mbd9-1*, and the complementary transgenic lines harboring WT and mutated *MBD9* transgenes. Values are mean ± SD. $^{**}P < 0.01$, Student's *t*-test.

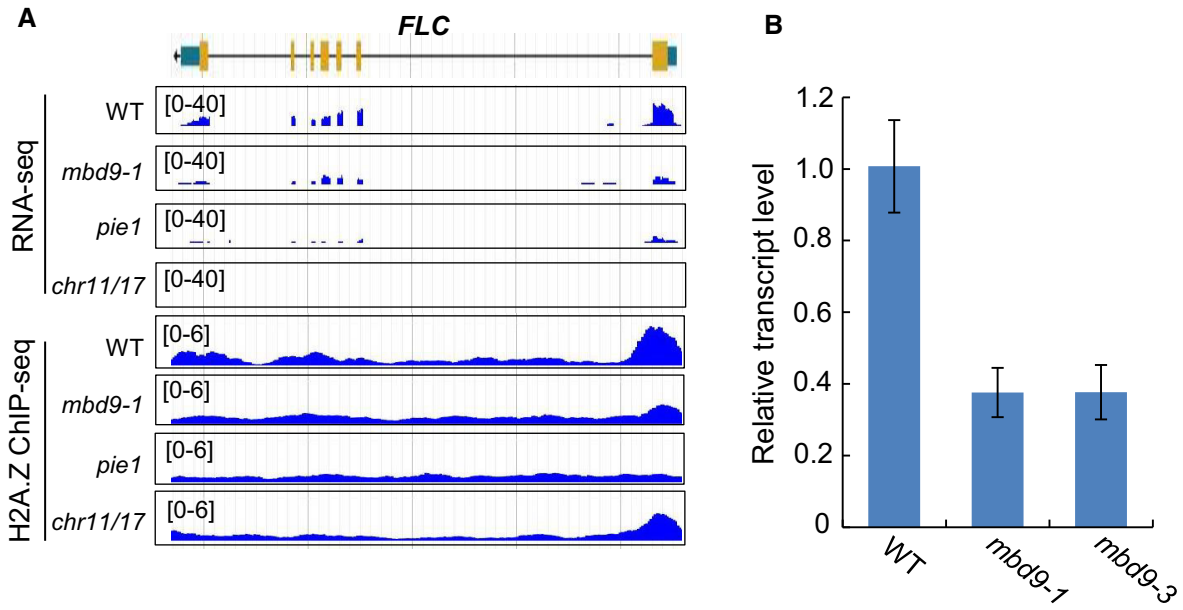

Figure EV5. The expression and H2A.Z enrichment of *FLC* in the WT, *mbd9-1*, *pie1*, and *chr11/17* mutants.

A Snapshots showing RNA-seq and H2A.Z ChIP-seq signals of *FLC* in WT, *mbd9-1*, *pie1*, and *chr11/17*.

B Determination of the transcript levels of *FLC* in WT, *mbd9-1*, and *mbd9-3* by RT-qPCR. Results shown are mean ± SD from three independent biological replicates.